Bioresources and Bioprocessing

RESEARCH

Open Access

Super-strong and high-performance electrical film heater derived from silver nanowire/aligned bacterial cellulose film

Guichun Hu[1,2], Amir Varamesh[1], Na Zhong[1], Fangong Kong[2] and Jinguang Hu[1*]

Abstract

High-performance electrical Joule heaters with high mechanical properties, low driving voltage, rapid response, and flexibility are highly desirable for portable thermal management. Herein, by using aligned bacterial cellulose (BC) and silver nanowire (AgNW), we fabricated a novel film heater based on Joule heating phenomena. The aligned BC film prepared by stretching BC hydrogel and hot-pressing drying technology showed outstanding mechanical properties and flexibility. The ultrahigh strength of up to 1018 MPa and the toughness of 20 MJ/m^3 were obtained for the aligned BC film with 40% wet-stretching (BC-40). In addition, the aligned BC film could be folded into desirable shapes. The AgNW was spray-coated on the surface of aligned BC-40 film and then covered with polydimethylsiloxane to form a P@AgNW@BC heater. P@AgNW@BC heater showed excellent conductivity, which endowed the film heater with an outstanding Joule heating performance. P@AgNW@BC heater could reach ~ 98 ℃ at a very low driving voltage of 4 V with a rapid heating response (13 s) and long-term temperature stability. The P@AgNW@BC heater with such an outstanding heating performance can be used as a flexible heating device for different applications in daily life like deicing/defogging device, wearable thermotherapy, etc.

Keywords Bacterial cellulose film, Silver nanowire, Joule heater, Mechanical strength, Flexibility

Graphical Abstract

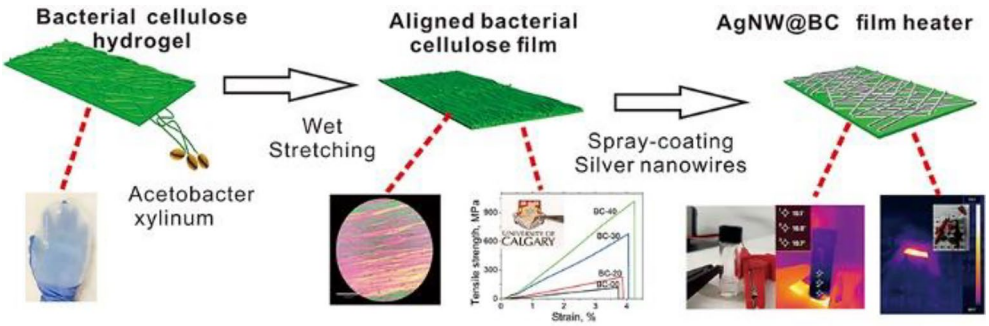

*Correspondence:
Jinguang Hu
jinguang.hu@ucalgary.ca
Full list of author information is available at the end of the article

Introduction

Electrical heaters based on the Joule heating effect have attracted significant attention from both academia and industry (Hossain et al. 2021; Veeramuthu et al. 2019). The high efficiency of electrical heaters in converting electricity into heat has led to widespread use of them for a variety of purposes in daily life, including snow-removal devices, local heating, deforesting and defogging, personal thermal management, healthcare thermotherapy, etc. (Meng et al. 2019). In light of the fast-growing and emerging need for electrical heaters, it is extremely important to develop electrical film heaters that fulfill the end-users demanding specifications. These include excellent mechanical properties, being flexible and shapable, having low driving voltage, satisfying heating temperature, rapid response, outstanding heating reliability, durability, and portability (Hossain et al. 2021; Wang et al. 2020). To achieve the above-mentioned characteristics, electrical heaters must have a well-designed structure.

Typically, electrical film heaters are fabricated by sputtering, coating, or printing conductive materials onto flexible substrates (Wu et al. 2022; Jyothibasu et al. 2019). Various conductive materials, such as polymers, metal nanowires, and carbon-based materials have been widely studied over the past several decades for fabrication of the film heaters (Yu et al. 2019; Zhang et al. 2018; Jia et al. 2018). Among these materials, silver nanowire (AgNW), has attracted considerable attention owing to its unique features, including high conductivity, considerable flexibility, and processability in aqueous dispersions (Ma et al. 2019; Zhou et al. 2020a, b). For example, Cheng et al. fabricated a cellulose nanofiber/silver nanowire nano paper electrical heater with an excellent heating temperature (~220 °C) (Cheng et al. 2022). As for the substrates in electrical heaters, many flexible membrane materials, such as petroleum plastic, paper, and natural polymer films have been used (Cao et al. 2019, 2020). Among various natural polymer films, cellulose film possesses many unique advantages, such as nontoxicity, biocompatibility, flexibility, and sustainability, which makes it a widely available and ideal candidate substrate for electrical film heaters (Kandhola et al. 2020; Song et al. 2019; Vallejo et al. 2021; Zhou et al. 2021;). Liang et al. fabricated a regenerated cellulose/silver nanowire composite film heater which achieves 107 ℃ at a voltage of 2 V and tensile strength of 61 MPa (Liang et al. 2020). Lu et al. prepared the cellulose/multiwalled carbon nanotube composite film with high Joule heating performance to reach 166 ℃ at the input voltage of 2.0 V and low tensile strength of 110 MPa (Lu et al. 2022). Zhou et al. fabricated cellulose nanofiber/MXene film with an outstanding and steady Joule heating performance to achieve more than 100 ℃ at 6 V voltage and mechanical strength of 112.5 MPa (Zhou et al. 2020a, b). These cellulose-based electrical heaters exhibit excellent Joule heating performances, but their mechanical properties are low and unsatisfying, which limits the application of cellulose-based electrical heaters.

Aerobic bacteria produces bacterial cellulose (BC) with randomly oriented fibrous network structure under static immersion. As compared with plant-based cellulose, BC fibers possess high specific surface area/purify/crystallinity/degree of polymerization, along with better biocompatibility (Zikmanis et al. 2021). In addition, the align BC film prepared by wet-stretching method shows excellent mechanical properties (Wang et al. 2018). In this work, we report a novel ultratough, flexible, and high-performance electrical heater derived from super-strong aligned BC film and highly conductive AgNW via a facile and efficient spray-coating method. The aligned BC film prepared by the wet-stretching and hot-pressing drying process exhibited high-record strength (1018 MPa) and excellent toughness (20 MJ m^{-3}). The flexible and ultrastrong aligned BC film acted as high-performance substrates and was spray-coated with AgNW to form AgNW@BC composite film. To avoid the AgNW oxidization, the AgNW@BC composite film was coated with polydimethylsiloxane (PDMS) to fabricate the P@AgNW@BC film heater. The P@AgNW@BC electrical film heater not only demonstrated superior mechanical robustness and flexibility, but also an outstanding Joule heating performance (up to at 98 ℃ at 4 V). The designed P@AgNW@BC electrical film is a promising candidate for applications in flexible electrical heaters in diverse areas.

Experimental

Materials

The BC was self-made at the in-house lab (University of Calgary, Canada). The $AgNO_3$, poly (N-vinyl-2-pyrrolidone) (PVP, molecular weight of 15,000), methanol, ethanediol (EG), glucose, yeast extract, peptone, sodium phosphate dibasic, citric acid, magnesium sulfate, NaCl and NaOH of analytical grade, polydimethylsiloxane (PDMS) and plasticizer were bought from Sigma Aldrich (Canada). *Acetobacter xylinum* (ATCC 23769) was purchased from American Type Culture Collection (USA). *Escherichia coli* (*E. coli,* ATCC 25922) was purchased from the American Culture Collection. All the chemicals were used as received without further purification.

BC films fabrication

Acetobacter xylinum was incubated with HS-medium (glucose 20 g/L, yeast extract 5 g/L, bacto-peptone 5 g/L,

sodium phosphate dibasic 2.7 g/L, citric acid 1.15 g/L, and magnesium sulphate 1.0 g/L) for 21 days in a static culture. Then BC membranes were boiled in 0.1 wt % NaOH for 60 min to get rid of the remaining HS-medium and microorganisms, and finally repeatedly rinsed with pure water until the filtrate became neutral.

The purified BC films were cut into a rectangular shape and measured its length which marked as the original length. Then the BC films were wet-drawn using a tensile tester (Series 1500, Qualitest) at a speed of 1 mm/min to reach a strain of 10%. Subsequently, the 10% wet-drawn BC films were unloaded from the tensile tester, shaken repeatedly, and further stretched to achieve a higher wet-drawing strain of 20%. Then, it has been unloaded and the last step was repeated to reach the wet-drawn strain of 30% and 40%. Finally, the BC film samples were press-dried at 60 ℃ for 24 h with the hot press machine (heat press machine, mg-h 10 t 35 v, DABPRSS Technologies, China). The range of wet-drawn strain (0%, 20%, 30%, and 40%) was selected based on (Wang et al. 2018). For comparison purpose, the pristine BC film (0%) was also prepared by hot-press drying at 60 ℃ for 24 h. The BC films with wet-drawn strain of 0%, 20%, 30%, and 40% were named BC-00, BC-20, BC-30, and BC-40, respectively.

Preparation of P@AgNW@BC composite film

Briefly, 60 ml of PVP/EG solution (0.18 mol/L) and 30 µL of NaCl aqueous solution (0.1 mol/L) were added into a flask and preheated at 150 ℃ in an oil bath for 60 min under stirring. Then, 30 ml of freshly prepared $AgNO_3$/EG solution (0.12 mol/l) was added dropwise to the flask under stirring and heated at 150 ℃ for another 240 min. After the reaction, the solution was cooled down at room temperature, then a large amount of methanol was added and the mixture was centrifuged (10,000 rpm/min, 10 min) six times to purify the silver nanowires (AgNWs). Finally, AgNWs were redispersed in methanol for the following application.

The dispersed AgNWs solution (10 mg/ml, 3 ml) was spray-coated onto the aligned BC-40 film (area size ~ 15 cm^2) using a Paasche airbrush (VL Siphon feed, 0.73 mm nozzle internal diameter, Paasche airbrush, USA), maintaining ~ 7 cm distance from spray nozzle to film and air bar at 1.6 bar. Then, the spray-coated aligned BC film (AgNW@BC) was successively dried under ambient conditions (10 min) and in 110 ℃ oven for 10 min. This process was, respectively, repeated 2, 3, 5, and 7 times to obtain AgNW@BC composite film with 2, 3, 5, and 7 AgNW layers. Finally, the AgNW@BC composite films were spin-coated with PDMS to obtain P@AgNW@BC composite film. The AgNW layers of P@AgNW@BC composite films varied in 2, 3, 5, and 7 were named P@AgNW@BC-2, P@AgNW@BC-3, P@AgNW@BC-5, and P@AgNW@BC-7, respectively.

Characterization

The morphological features of the samples were examined using a field emission scanning electron microscope (SEM, JSM-6700F, JEOL, Japan). The wide-angle X-ray diffractogram (XRD) was acquired on an X-ray diffractometer (D/max-2500, Rigaku Denki, Japan) at the scanning speed of 2°/min. The Olympus BH-2 optical microscope was used to observe the aligned BC films with the assistance of two polarized light filters. Mechanical performances of the original and wet-stretching BC films in the path of the wet-stretching were investigated on the tensile tester (Series 1500, Qualitest) at a speed of 1 mm/min and each samples tested 3 times. Young's modulus was acquired as the slope at low strain and toughness was determined as the area under the stress–strain curve. Light transmittance of the samples was measured using a visible spectrophotometer (CARY 50 Bio, Varian) with a wavelength range of 380 to 730 nm. The sheet resistance was measured using a four-point probe tester (2258C, Suzhou Lattice Electronics Co., Ltd., China). The electric heating performance of the sample was characterized under a constant applied voltage of 1–7 V and current of 2 A with an infrared camera (FLIR A300, FLIR Systems, USA) and sourcemeter (2400, Keithley, USA).

Antibacterial testing

The antimicrobial activities of P@AgNW@BC films were analyzed by inhibition zone testing. *Escherichia coli* (*E. coli*) is a Gram-negative, rod-shaped bacterium found in lower intestine of warm blooded organisms (endotherms). Due to its strong ability to survive in nature, it also can be found in skin and is often used to measure the antibacterial properties of electrical heater (Gupta et al. 2013; Zhu et al. 2022; Du et al. 2022) So, *E. coli* was used to test the antibacterial activity of P@AgNW@BC films. *E. coli* was cultivated in 10 ml Mueller–Hinton Broth (Cation adjusted) at 37 ℃ for 12 h. Then, 150 µl *E. coli* suspension (4.5×10^6 CFU/ml) was uniformly spread over a Luria–Bertani agar plate. Samples were carefully placed on the center of the agar plate and incubated in a constant temperature incubator at 37 ℃ for 24 h. The image of the suppression area

was taken by a ChemiDoc Imaging System (Bio-RAD ChemiDocTM MP Imaging System, UK).

Results and discussion

Fabrication strategy and structural characterization of aligned BC film

The pristine BC nanofibrils extruded by *Acetobacter xylinum* are randomly distributed in a wet membrane and then the wet nanofibril membrane was stretched to form BC film with the aligned cellulose nanofibrils (shown in Fig. 1a). BC film's wet-stretching percentage is defined as the ratio between the value of the stretching-induced length and the original length. The polarized optical microscopy images of the BC film with different wet-stretching percentages are shown in Fig. 1b–e. The pristine BC film (BC-00) exhibited randomly distributed brightly colored regions. However, colorful discontinuous strips were observed in the BC film with 20% wet-stretching (BC-20) indicating elongation of the cellulose fibril crystalline domains with the wet-stretching direction. As the wet-stretching percentage increased to 30% (BC-30), the colorful strips became more pronounced. This progression of colours was consistent with increasing alignment, as shown in the BC film with a 40% wet-stretching percentage (BC-40).

The surface morphologies of BC films with different wet-stretching percentages were also investigated by field emission scanning electron microscope (FE-SEM) as shown in Fig. 2. The original BC-00 film contains randomly distributed nanofibrils, while the BC-20 film showed an increasing amount of aligned nanofibrils. After further increasing the wet-stretching percentage to 30%, more aligned nanofibrils of BC-30 were observed. For the BC-40 film, there were few wrinkles parallel to each other, showing a well-aligned structure on a micro-scale. In the cross-section morphology of the pristine BC-00, a layered structure was apparent in the pristine BC-00 film. However, the cross-section morphology of the BC-40 film showed some obvious fibril bundles, which was also observed in accordance with the literature results (Wang et al. 2018). This observation is assumed to be related to the formation of strong hydrogen bonding between the highly aligned nanofibrils (Wu et al. 2020; Wang et al. 2018).

The light transmittances of the different BC films are depicted in Fig. 3a. Both the original and stretched films show high transmittance covering the entire visible wavelength ranging from 380 to 730 nm. The light transmittance slightly decreased with the increase of the wet-stretching percentage of BC films. The transmittances of the BC films were incredibly high with transmittances of above 88% at 550 nm. The University of Calgary logo covered with BC-40 film could be clearly observed in Fig. 3a, which further indicated the high transmittance of BC films.

The microstructural changes of BC films were investigated by XRD (Fig. 3b). BC films with different wet-stretching percentages showed significant diffraction

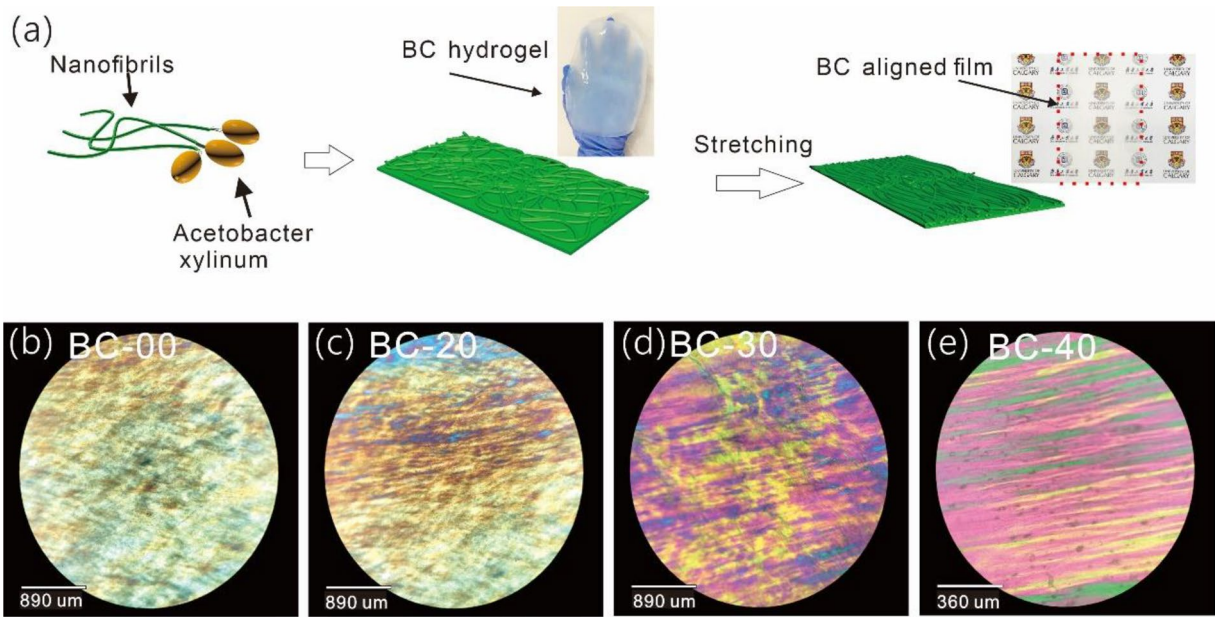

Fig. 1 **a** The schematic illustration of wet-stretching BC film fabrication; **b–e** polarized optical microscopy image of BC films with different wet-drawing **b** BC-00, **c** BC-20, **d** BC-30, and **e** BC-40

peaks at 14.6°, 16.3° and 22.5° with a slightly distinguishable difference in their intensities. The peaks were indexed to the (100), (010) and (110) crystallographic planes of cellulose Iα, respectively, as reported in the previous studies (Zikmanis et al. 2021). BC-40 and BC-30 showed higher intensities at the (100) and (110) angles, proving that they pose highly crystalline structures. From their crystallinity and the wet-stretching percentage, it can be concluded that the wet-stretching improves the crystallization of BC film.

The tensile strength and toughness of BC films that undergo different stretching levels were tested (Fig. 3c, Table 1). Interestingly, a higher wet-stretching strain level led to an increase in strength and modulus along with improved toughness. The tensile strength of the original BC-00 film was 116.5 MPa. When it stretched to 20%, the aligned BC-20 film showed a significantly improved

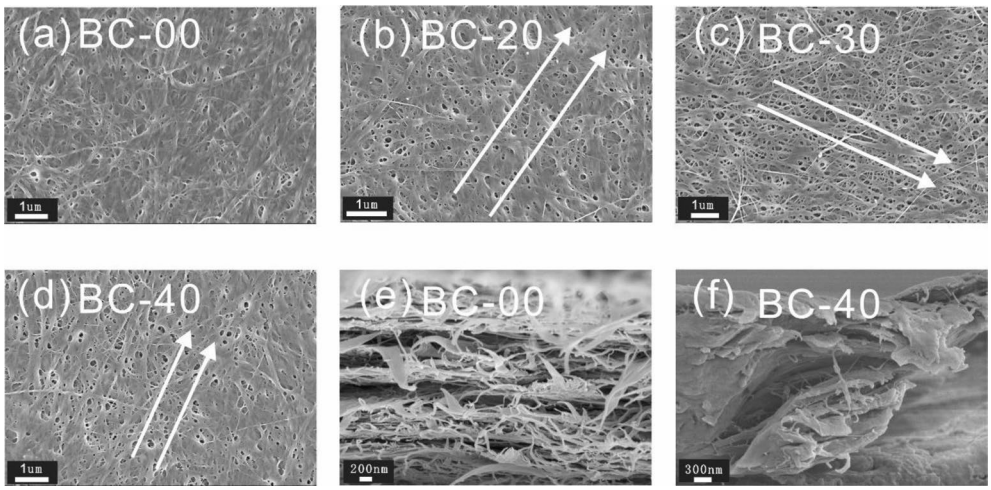

Fig. 2 SEM images of the surface of **a** BC-00, **b** BC-20, **c** BC-30, and **d** BC-40 wet-stretching BC films; **e–f** cross-sectional images of **e** BC-00 film and **f** BC-40 film

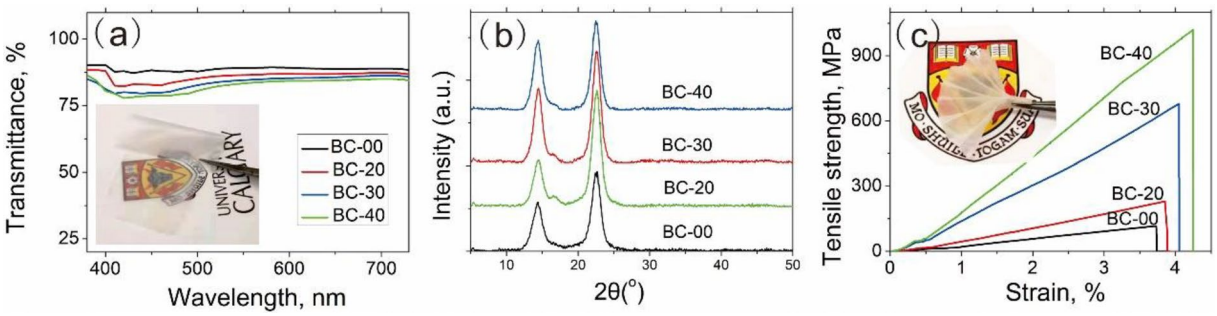

Fig. 3 **a** Transmittance, **b** XRD and **c** tensile strength of BC films with different wet-stretching

Table 1 Mechanical properties of BC films with different wet-stretching

Samples	Strain at the break, %	s.d.	Young's modulus, GPa	s.d.	Tensile strength, MPa	s.d.	Toughness, MJ/m^{-3}	s.d.
BC-00	3.7	0.075	9.2	1.5	116.5	8.0	2.0	0.6
BC-20	3.8	0.05	12.3	1.0	229.9	6.0	4.0	0.3
BC-30	4.0	0.06	41.1	0.9	678.5	6.6	12.7	0.4
BC-40	4.2	0.075	43.6	0.7	1018.8	5.3	20.2	0.4

s.d. stands for standard deviation

tensile strength (229.9 MPa) as well as toughness (4.0 MJ/m), which were 1.9 times and 2.0 times higher than the original one, respectively. The exceptional mechanical properties of the BC films were associated with highly crystalline cellulose from bacterial biosynthesis (Wu et al. 2020; Wang et al. 2018). The mechanical properties of the BC film were further enhanced with increasing structural alignment. As the wet-stretching strain increased to 40%, the tensile strength reached 1018.8 MPa, and Young's modulus increased to 20.2 MJ/m^3. The increase in Young's modulus indicates the reduction of the cellulose film deformation. The reason for the superb mechanical properties of our BC film is due to the wet stretching-induced nanoscale alignment of the nanofibrils and densely packed microfibril bundles. As shown SEM images (Fig. 2), the BC film fabricated after high wet-stretching percentage (e.g., BC-40) showed a well-aligned nanofibril structure. According to FTIR spectrograms (Additional file 1: Fig. S1), the characteristic vibrational modes of BC films after different wet-stretching percentages were almost same in the typical fingerprint regions as reported earlier (Daya et al. 2013; Shibayama et al. 1990). The characteristic peaks located at 3500–3100, 1430, 1111, 1046, and 892 cm-1 were assigned to O–H, CH_2, C–C, C–O–H, and C–O–C groups, respectively. (Daya et al. 2013) have reported that signals near 892 and 1430 are designated as an "amorphous" band and "crystallinity" band, respectively. The intensities of BC-30-BC-40 at 1430 cm^{-1} obviously increased compared with BC-00. The intensities of BC films at 892 cm^{-1} are almost no change. This phenomenon is coincided with the results of XRD of BC films indicating the improvement of crystallization of BC film after the wet-stretching. In addition, the densities of BC films (Additional file 1: Fig. S2) enhanced with the increase of wet-stretch percentage, indicating the strong interaction among the cellulose nanofibers. Similar results have also been observed and studied by others (Wang et al. 2018; Wu et al. 2020). For example, Wang et al. (Wang et al. 2018) investigated the underlying mechanism of the superb mechanical properties of the highly aligned BC film with molecular dynamics simulations and found that the well-aligned model exhibits both strength and toughness that are exceptionally higher than those of the randomly aligned model. In addition, the wet-stretching BC-40 film was extremely foldable and could be folded into a paper fan (Fig. 3c). Upon unfolding, the BC film did not show visible degradation and the tensile strengths of BC films after folding 100 times (Additional file 1: Figs. S3, S4) showed no obvious change, indicating its tough and flexible properties.

Electrical conductivity of AgNW@BC film

Silver nanowires (AgNW) were synthesized by a polyol process which was based on the reduction of an inorganic salt by a polyol at an elevated temperature. In this method, EG was used as both solvent and reducing agent, PVP was utilized as stabilizing agent, and $AgNO_3$ was used as Ag source. According to the UV–vis absorption spectrum of the AgNWs solution (Fig. 4a), there were two narrow peaks at 380 nm and 350 nm. According to previous studies (Yang et al. 2013; Zhang et al. 2019; Tang et al. 2009), the existence of the absorption peaks at 350/380 and 410 nm in the UV–vis spectrum is the characteristic peaks of long AgNWs and silver nanoparticles, respectively. Hence, the absence of the absorption peak at 410 nm in Fig. 4a also verified the high purity of the prepared AgNWs. The UV spectra were unanimous with the SEM images (shown in Fig. 4b–c) which display the size of AgNW. It is noticeable that there were mainly AgNWs with an average length of 2–3 um, besides very few silver nanoparticles observable, showing the high purity of AgNWs. In addition, there is an aggregation of the AgNWs as shown in Fig. 4b probably due to the overlap of the AgNW solution droplets.

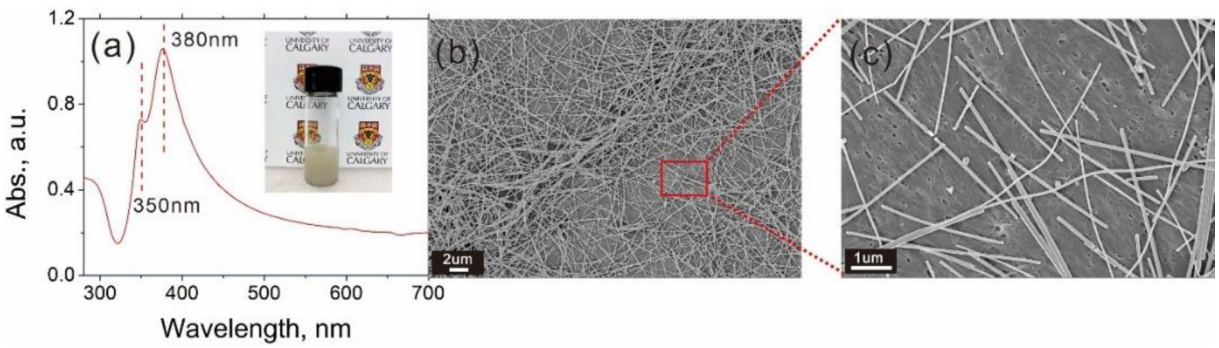

Fig. 4 **a** The UV absorbance of AgNW solution; **b–c** SEM images of silver nanowires on BC-40 at **b** lower and **c** higher magnifications

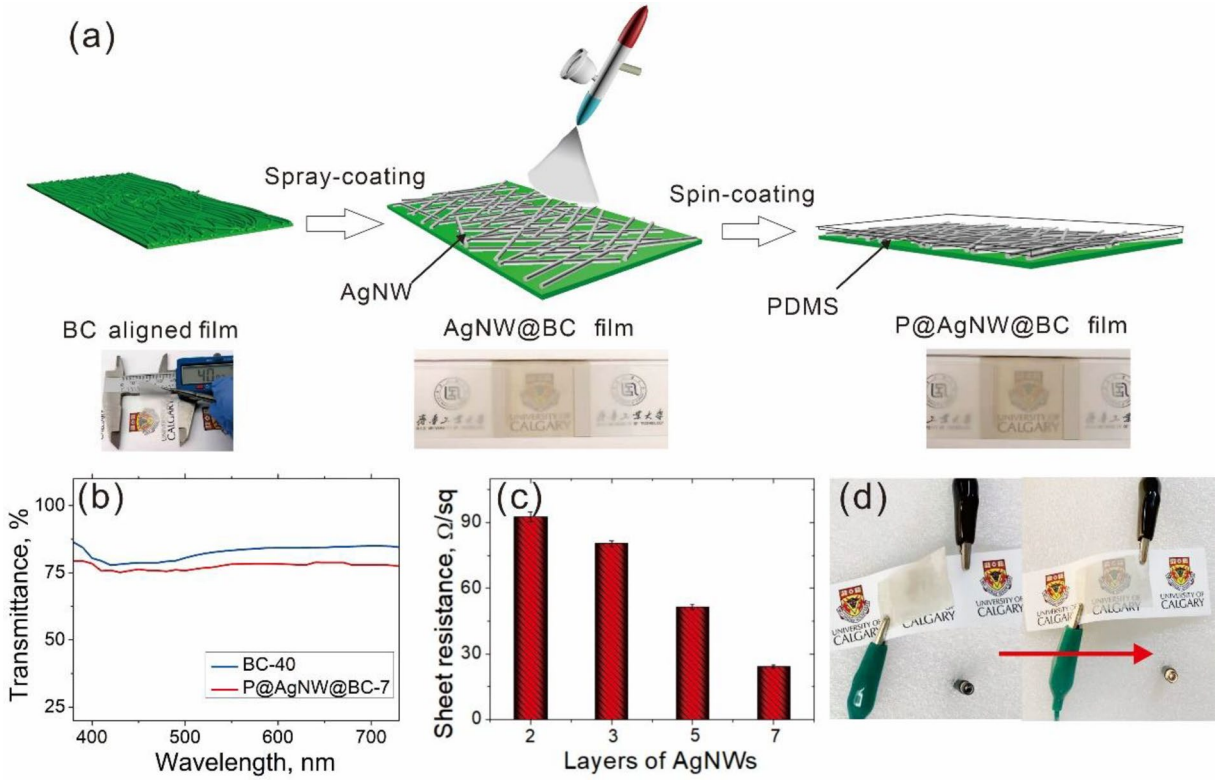

Fig. 5 **a** Schematic illustration of the fabrication process of P@AgNW@BC composite film; **b** transparent of the BC-40 film and P@AgNW@BC-7 film; **c** the square resistance of P@AgNW@BC-7 film with different spray-coating layers; **d** photographs of series-wound white light-emitting diodes (LEDs) and conductive P@AgNW@BC-7 film

The BC-40 film was spray-coated with AgNWs and dried in atmosphere. Then spin-coated with PDMS to form P@ AgNW@BC composite film as schematically depicted in Fig. 5a. The BC-40 film showed transparency, whereas, P@AgNW@BC-7 had very small change detectable by the naked eye, as noted by the photography of University Logo covered with P@AgNW@BC-7 (Fig. 5a). Figure 5b reveals that BC-40 film poses excellent transparency with transmittance values of 88% at 550 nm and 89% at 700 nm in the UV–Vis region. However, P@AgNW@BC-7 film has a slight diminution, but it is still very acceptable, with transparency of 79% at 550 nm and 80% at 700 nm, respectively. AgNW solution are not completely transparent and shows absorption in the visible region (400–780 nm) (shown in Fig. 4a), thus the AgNWs layers spray-coated on the BC film lead to the decrease transparency of P@AgNW@BC-7.The electrical properties of P@AgNW@BC film were optimized by adjusting the AgNW layers. When the number of AgNW layers increased, the sheet resistance significantly reduced from 92 to 51 Ω/sq. A minimum sheet resistance value of 23 Ω/sq was observed for the seven-layered AgNWs (P@AgNW@BC-7). Figure 5d presents the luminance of a white LED, in a series circuit with the P@AgNW@BC at a power supply of 3 V. The white LED is lighted as the P@AgNW@BC-7 film attached.

Joule heating performance of P@AgNW@BC film

A high level of electrical conductivity is crucial during the design of electric heaters in order to ensure good heating performance. The time-dependent temperature changes of P@AgNW@BC samples were determined under different voltages on the range of 1–7 V (Fig. 6a–d). The saturation temperatures in all P@AgNW@BC samples increased with the rise of the driving voltage. For P@AgNW@BC-2, the saturation temperature rose from 30 ℃ to 45 ℃ as the driving voltage increased from 1 to 7 V (Fig. 6a). The P@ AgNW@BC sample with high AgNW content was easy to achieve the high saturation temperature at the same driving voltage and required to obtain a similar saturation temperature at a low driving voltage. A saturation temperature of 40 ℃

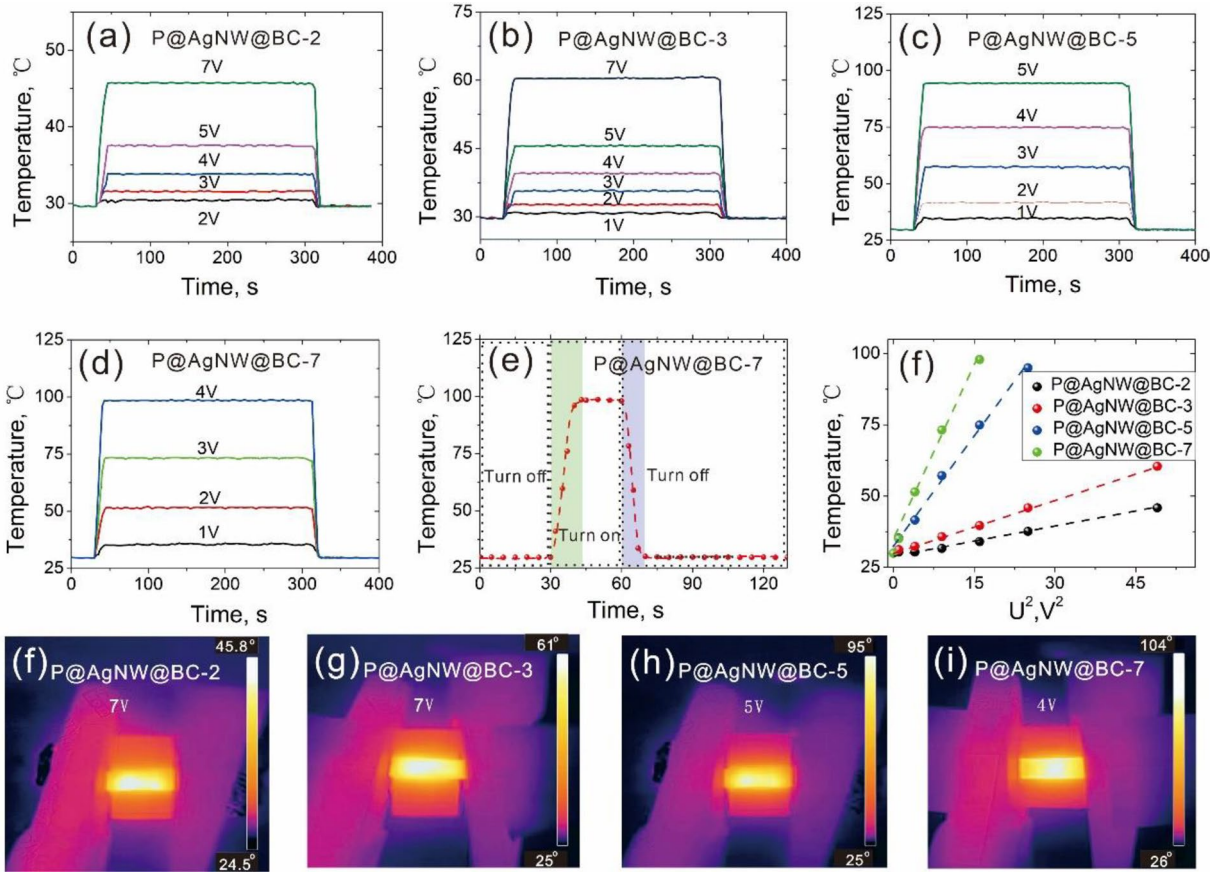

Fig. 6 **a–d** Time-dependent temperature change of the P@AgNW@BC composite film with different AgNW spray-coating layers under different applied voltages; **e** the heating and cooling rates of P@AgNW@BC-7 film heater at 4 V; **f–i** infrared images of P@AgNW@BC film heaters with various driving voltages

was obtained at 4 V for P@ AgNW@BC-3, whereas higher saturation temperatures of 75 ℃ and 98 ℃ were achieved at 4 V for P@AgNW@BC-5 and P@ AgNW@BC-7, respectively (Fig. 6b–d). Besides a saturation temperature of 45 ℃ was gained at 7 V for P@ AgNW@BC-2, while a saturation temperature of 57 ℃ is reached at only 3 V for P@ AgNW@BC-5. Moreover, a saturation temperature of 51 ℃ was achieved at an even lower voltage of 2 V for P@AgNW@BC-5. It was interesting to observe that, regardless of the applied voltage, our P@AgNW@BC samples respond very quickly to heating-up processes. As shown in Fig. 6e, when the voltage was applied to the P@ AgNW@BC-7 composite film, its temperature increased rapidly and then reached a saturated value within 13 s. Once the input voltage was switched off, the films cooled down quickly. The heating stability and repeatability of a heater are also important for its practical applications. As shown in Additional file 1: Fig. S5, cyclic heating/cooling was conducted on P@AgNW@BC-7 film heater with on/off switch of driving voltage. The surface temperature steadily increased and decreased during repeated driving voltage for > 200 cycles and the maximum value of the surface temperature was basically the same as the driving voltage both at 2 V and 4V, which indicated the good heating stability and repeatability of P@AgNW@BC-7 film. Figure 6f shows the saturation temperature of the P@ AgNW@BC films corresponding to different drive voltages. According to the energy balance principle, the time-dependent thermal model is developed as (Wang et al. 2020):

$$T = T_0 + \frac{U^2}{RhA}\left(1 - e^{-\left(\frac{hA}{mc}\right)}\right)t,$$

where U stands for driving voltage, R is the resistance of the electrical heater, m represents the mass, A is the area, c is the specific heat capacity, h stands for convective heat-transfer coefficient, T stands for the temperature of the electrical heater and T_0 is the initial ambient temperature. The saturation temperatures of the P@AgNW@BC film heaters (Fig. 6f) showed a highly correlated

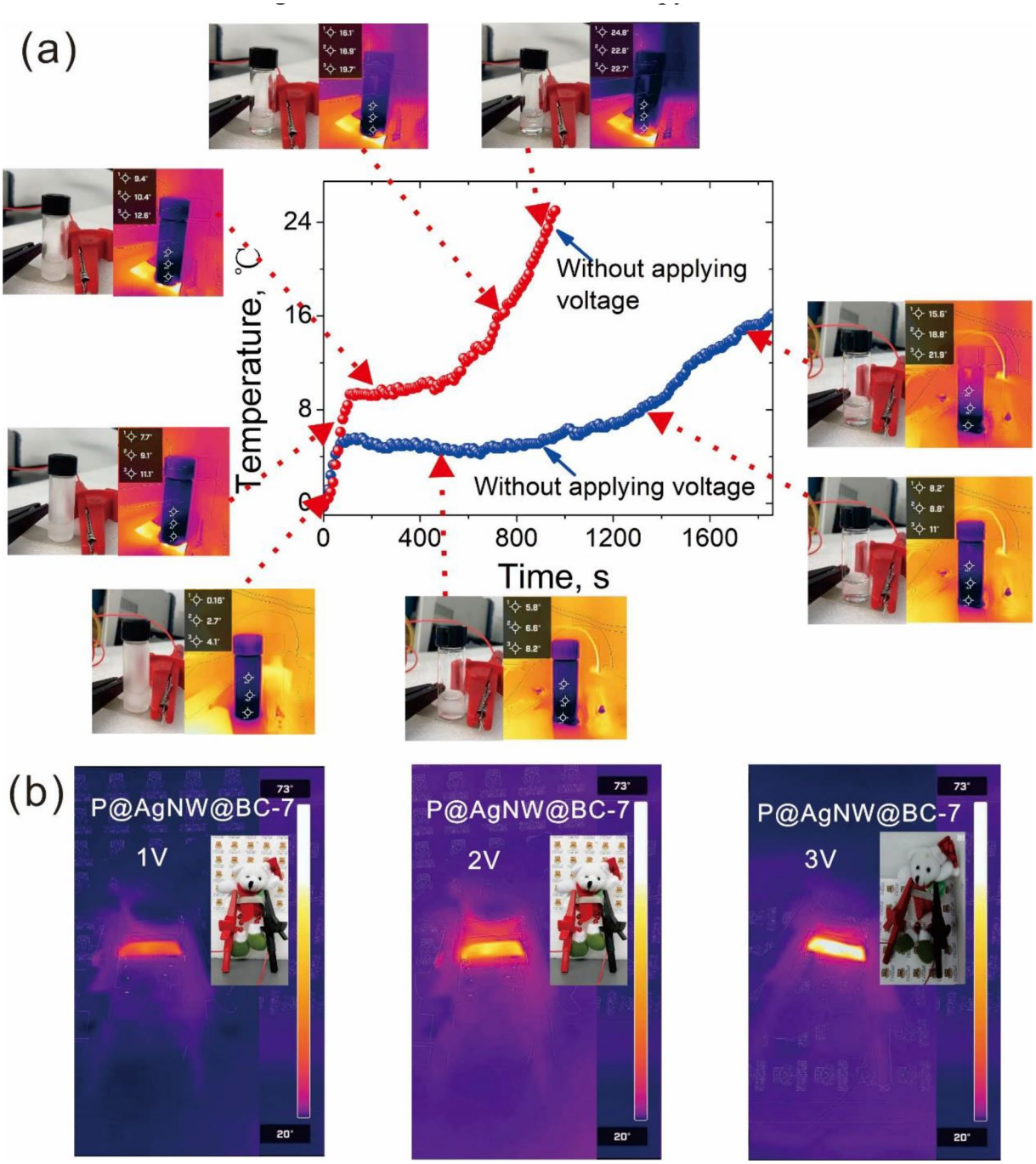

Fig. 7 **a** The photographs of deicing device prepared with P@AgNW@BC-7; **b** IR thermal images of P@AgNW@BC-7 wearable thermotherapy at driving voltage of 1 V, 2 V, and 3 V

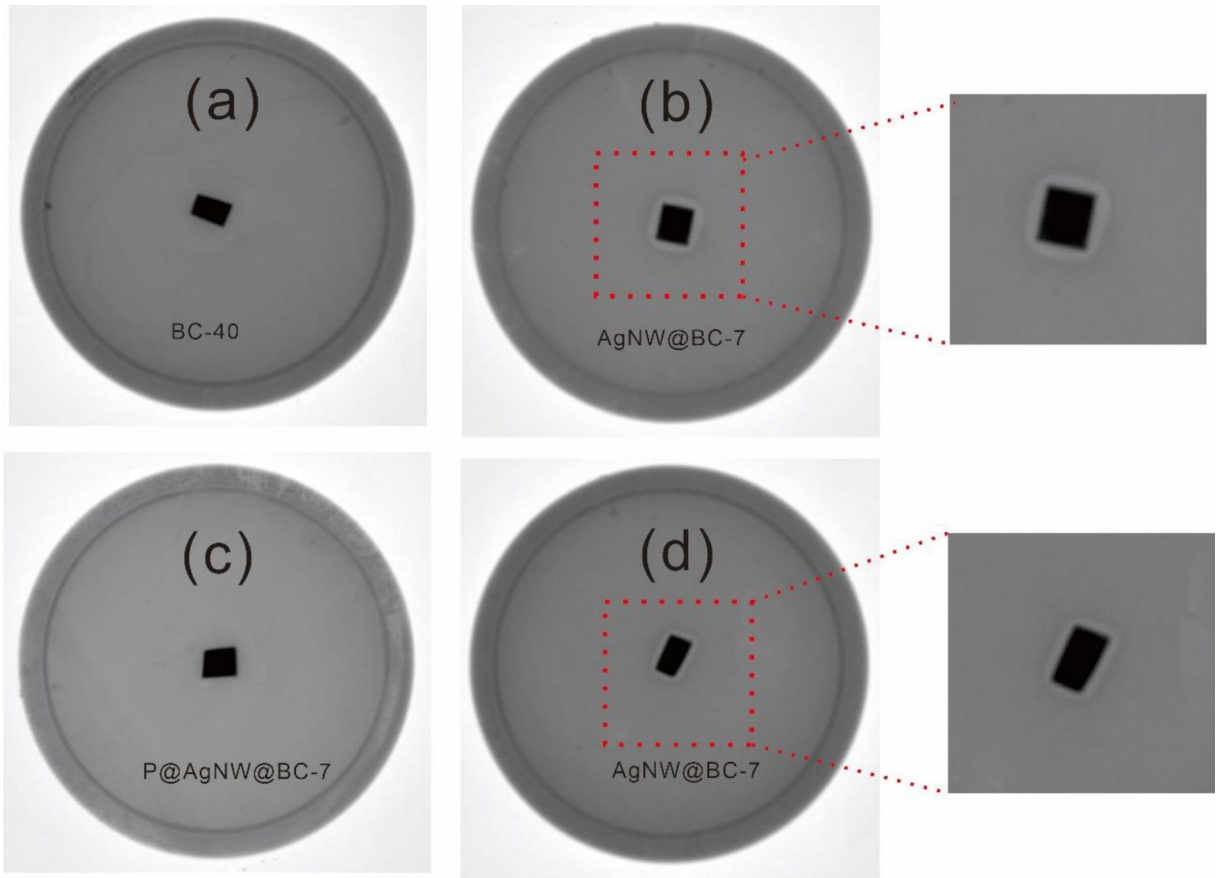

Fig. 8 Photographs of *E. coli* cultivated on agar plates for **a** BC-40 film, **b** AgNW@BC-7 film, **c** P@ AgNW@ BC-7 film, **d** AgNW@ BC-7 film stored for 1 year

linear relationship with the square of the applied voltage (U^2), confirming the precision of the theoretical prediction model of saturation temperature at different applied voltages. With constant driving voltage, the heaters with higher AgNW content showed higher saturation temperatures due to reduced electrical resistance. The above results together with the specific switchable characteristics demonstrate that the heating performance of the heaters could be easily adjusted by controlling the AgNW contents or driving the voltage. Furthermore, The Joule heating performances of the P@AgNW@BC film heaters were investigated at various driving voltages, and the temperature was monitored using an FTIR camera as shown in Fig. 6f–i. Obviously, the thermal images present a uniform temperature distribution, which is regarded as an important criterion in electrical heaters.

The low driving voltage ensured the safety of the devices for the human body, while the fast thermal response made the devices reach the desired temperature rapidly. And the wide temperature range endowed the devices with versatile applications. Based on the superior Joule heating performance and high stability, an electric deicing device and a wearable heater had been fabricated by using the P@AgNW@BC-7 film. A simple deicing device (Fig. 7a) was fabricated with a 10 mm width and 40 mm length, which was driven at 4 V. An ice cube (about 1.0 g water) in a glass bottle melted quickly and transferred completely to the liquid phase within 540 s at 3.0 V. During this process, the temperature of the bottom water increased from original − 0.5 ℃ to 8 ℃. More importantly, the water temperature increased to about 25 ℃ via electric heating for another 200 s. As a control, the ice cube without electric heating melted slowly and did not melt completely until 800 s. Figure 7b shows the application of P@AgNW@BC-7 film as an electrical hater in wearable thermotherapy. The P@AgNW@BC-7 film affixed to the chest of a doll was heated up by using different driving voltages from ambient temperature to 35 ℃,

51 ℃, and 73 ℃. This observation shows the great applicability of the developed film in-medical thermotherapy to effectively relieve pain and stiffness within the temperature range of 30–77 ℃. Therefore, the P@AgNW@BC-7 films could successfully be used to construct low-voltage driving devices, such as deicing devices, wearable thermotherapy, and so on.

The antibacterial properties of P@AgNW@BC film

The antibacterial activity is imperative for the commercialization of thermal management film in many applications specifically those that are related to humans. It has been shown that silver nanowires pose excellent antibacterial properties (Zhou et al. 2021). To explore the antibacterial properties of different prepared films, the antibacterial activities of BC-40, AgNW@BC-7 (AgNW@BC film with 7 AgNW layers), and P@ AgNW@BC-7 films were tested against *E. coli* (ATCC 8739), as shown in Fig. 8. The pristine BC-40 film did not show antibacterial activity (Fig. 8a), whereas the AgNW@BC-7 film yielded good antibacterial performance against *E. coli* (Fig. 8b). This performance originated from the presence of AgNW in the BC film due to the antibiotic activity of AgNW. However, the mechanisms of the antibiotic activity of silver nanomaterials (silver nanowire and silver nanoparticle) are not well established to date and is still a topic of hot debate. Several mechanisms have been proposed (Li et al. 2010; Singh et al. 2016; Vanlalveni et al. 2021). For example, silver nanomaterials bind strongly with phosphorus and sulfur of the extracellular and intracellular membrane proteins, thus affects the cell respiration, replication and the lifetime of the cell. Besides, the interaction between the positively charged Ag ion with the negatively charged cell membranes led to the disruption of the cell morphology and the cell leakage leading to cell death. Apart from that, silver nanomaterials can also bind with the thiol and amino groups of membrane protein resulting in the formation of reactive oxygen species, which inhibits the cell respiration. It has also been suggested that the interaction of silver nanomaterials with cell wall increases the membrane permeability of forming pores or pits and thereby causing the death of bacteria (Morones et al. 2005; Yu and Yam 2004;). As our expected, the P@ AgNW@BC-7 film does not show antibacterial activity (Fig. 8c). The possible reason is that the PDMS covered the AgNW surface of P@AgNW@BC-7 film prohibited the oligodynamic effect of Ag. In addition, it is interesting to note that after one year of storage in the paper envelope placed in ambient environment, the AgNW@BC-7 film still showed excellent antibacterial performance (Fig. 8d).

Conclusions

In summary, we reported the fabrication P@AgNW@BC film heater with ultrahigh mechanical properties, flexibility, and excellent Joule heating performance. In detail, the aligned BC film was produced and used as a substrate to spray-coated with AgNWs and then spin-coated with PDMS to fabricate the P@AgNW@BC film heater. Wet-stretching and hot-press drying were used to prepare the aligned BC film with cellulose nanofibers. The mechanical properties of the aligned BC film substantially increased with the increase of wet-stretching. The BC-40 film with 40% wet-stretching exhibited ultrahigh strength of 1018 MPa and excellent toughness of 20 MJ m^{-3}. In addition, the aligned BC film showed great flexibility that could be shaped to any desired shape. The P@AgNW@BC film heater generated a hot saturation temperature of up to 98 ℃ at 4 V and exhibited a shorter response time (13 s) and long-term stability of saturation temperature. In addition, the AgNW@BC film showed outstanding antibacterial properties even after 1 year of storage. The P@ AgNW@BC film heater with such an excellent performance can be used as portable thermal management such as deicing, defogging, defrosting devices, wearable thermotherapy, etc.

Supplementary Information

The online version contains supplementary material available at https://doi.org/10.1186/s40643-023-00669-w.

Additional file 1: Fig. S1. FTIR spectra of BC films with different wet-stretching: **a** spectra from 550 to 4000 cm^{-1} **b** spectra from 550 to 1500 cm^{-1}. **Fig. S2.** The density of BC films with different wet-stretching. **Fig. S3.** The schematic diagram of the BC film fold and unfold. **Fig. S4.** The tensile strength of BC films after folding 100 times (BC-00-F, BC-20-F, BC-30-F, and BC-40-F represent the BC-00, BC-20, BC-30, and BC-40 after folding 100 times). **Fig. S5.** Heating stability and repeatability of the P@AgNW@BC-7 film heater upon repeated driving voltages.

Acknowledgements

We also thank the University of Calgary's Canada First Research Excellence Fund (CFREF) program, entitled the Global Research Initiative for Sustainable Low-Carbon Unconventional Resources (Canada) for supporting this project.

Author contributions

GH and AV—conceptualization, investigation, methodology, writing original draft and writing review and editing. NZ and FK—writing review and editing, analysis, and suggestion. JH—validation, resources, data curation, supervision, project administration, writing—review and editing, and funding acquisition.

Funding

This study was supported by the Key Laboratory of Auxiliary Chemistry and Technology for Chemical Industry, Ministry of Education (Grant No. KFKT2019-03) and the Foundation (No. ZR20190108) of the State Key Laboratory of Biobased Material and Green Papermaking, Qilu University of Technology, Shandong Academy of Sciences. The authors are also grateful for the support of the National Natural Science Foundation of China (Grant No. 31971605) and

the Natural Science Foundation of Shandong (No. ZR2020MC156). Canada Frist Research Excellent Fund.

Availability of data and materials
Will be provided based on request.

Declarations

Ethics approval and consent to participate
Not applicable.

Consent for publication
Not applicable.

Competing interests
The authors declare that they have no competing interests.

Author details
[1]Department of Chemical & Petroleum Engineering, Schulich School of Engineering, Calgary, AB T2N 1N4, Canada. [2]State Key Laboratory of Biobased Material and Green Papermaking, Faculty of Light Industry, Shandong Academy of Sciences, Qilu University of Technology, Jinan 250353, People's Republic of China.

Received: 28 February 2023 Accepted: 21 July 2023
Published online: 23 August 2023

References

Cao WT, Ma C, Mao DS, Zhang J, Ma MG, Chen F (2019) MXene-reinforced cellulose nanofibril Inks for 3D-printed smart fibres and textiles. Adv Funct Mater 29:1905898

Cao J, Zhou Z, Song Q, Chen K, Su G, Zhou T, Zheng Z, Lu C, Zhang X (2020) Ultrarobust Ti3C2Tx MXene-based soft actuators via bamboo-inspired mesoscale assembly of hybrid nanostructures. ACS Nano 14:7055–7065

Cheng R, Wang B, Zeng J, Li J, Xu J, Gao W, Chen K (2022) High-performance and rapid-response electrical heaters derived from cellulose nanofiber/silver nanowire nanopapers for portable thermal management. ACS Appl Mater Interfaces 14:30144–30159

Dayal MS, Goswami N, Sahai A, Jain V, Mathur G, Mathur A (2013) Effect of media components on cell growth and bacterial cellulose production from *Acetobacter aceti* MTCC 2623. Carbohyd Polym 94:12–16

Du P, Zhang J, Guo Z, Wang H, Luo Z, Fan Z, Li B, Cai Z, Ge F (2022) A novel breathable flexible metallized fabric for wearable heating device with flame-retardant and antibacterial properties. J Mater Sci Technol 122:200–210

Gupta A, Maheshwari DK, Khandelwa G (2013) Antibacterial activity of *Glycyrrhiza glabra* roots against certain gram-positive and gram-negative bacterial strains. J Appl Natl Sci 5(2):459–464

Hossain M, Sibin KP, Rao KDM (2021) Angled-stencil lithography-based metal mesh/Ti3C2Tx MXene hybrid transparent electrodes for low-power and high-performance wearable thermotherapy. J Mater Chem C 9:6257

Jia L-C, Sun W-J, Zhou C-G, Yan D-X, Zhang Q-C, Li Z-M (2018) Integrated strength and toughness in graphene/calcium alginate films for highly efficient electromagnetic interference shielding. J Mater Chem C 6:9166–9174

Jyothibasu JP, Kuo D-W, Lee R-H (2019) Flexible and freestanding electrodes based on polypyrrole/carbon nanotube/ cellulose composites for supercapacitor application. Cellulose 26:4495–4513

Kandhola G, Djioleu A, Rajan K, Labbe N, Sakon J, Carrier DJ, Kim J-W (2020) Maximizing production of cellulose nanocrystals and nanofibers from pre-extracted loblolly pine kraft pulp: a response surface approach. Bioresour Bioprocess 7:19

Li WR, Xie XB, Shi QS, Zeng HY, OU-Yang YS, Chen YB (2010) Antibacterial activity and mechanism of silver nanoparticles on *Escherichia* coli. Appl Microbiol Biotechnol 85:1115–1122

Liang C, Ruan K, Zhang Y, Gu J (2020) Multifunctional flexible electromagnetic interference shielding silver nanowires/cellulose films with excellent thermal management and joule heating performances. ACS Appl Mater Interfaces 12:18023–18031

Lu H, Xia Z, Mi Q, Zhang J, Zheng X, He Z, Wu J, Zhang J (2022) Cellulose based conductive films with superior Joule heating performance, electromagnetic shielding efficiency and high stability by in situ welding to construct a segregated MWCNT conductive network. Ind Eng Chem Res 61:1773–1785

Ma Z, Kang S, Ma J, Shao L, Wei A, Liang C, Gu J, Yang B, Dong D, Wei L, Ji Z (2019) High-performance and rapid-response electrical heaters based on ultraflexible, heat-resistant, and mechanically strong aramid nanofiber/Ag nanowire nanocomposite papers. ACS Nano 13:7578–7590

Meng X, Chen T, Li Y, Liu S, Pan H, Ma Y, Chen Z, Zhang Y, Zhu S (2019) Assembly of carbon nanodots in graphene-based composite for flexible electro-thermal heater with ultrahigh efficiency. Nano Res 12:2498–2508

Morones JR, Elechiguerra JL, Camacho A, Holt K, Kouri JB, Ramírez JT, Yacaman MJ (2005) The bactericidal effect of silver nanoparticles. Nanotechnology 16:2346–2353

Shibayama M, Yamamoto T, Xiao C-F, Sakurai S, Hayami A, Nomura S (1990) Bulk and surface characterization of cellulose/poly(vinyl alcohol) blends by Fourier-transform infra-red spectroscopy. Ploymer 32(6):1010–1017

Singh D, Rawat D (2016) Microwave-assisted synthesis of silver nanoparticles from *Origanum majorana* and *Citrus* sinensis leaf and their antibacterial activity: a green chemistry approach. Bioresour Bioprocess 3:14

Song K, Zhu X, Zhu W, Li X (2019) Preparation and characterization of cellulose nanocrystal extracted from *Calotropis* procera biomass. Bioresour Bioprocess 6:45

Tang X, Tsuji M, Jiang P, Nishio M, Jang SM, Yoon SH (2009) Rapid and high-yield synthesis of silver nanowires using air-assisted polyol method with chloride ions. Colloids Surf Pysicochem Eng Aspects 338:33–39

Vallejo M, Cordeiro R, Dias PAN, Moura C, Henriques M, Seabra IJ, Malca CM, Morouco P (2021) Recovery and evaluation of cellulose from agroindustrial residues of corn, grape, pomegranate, strawberry-tree fruit and fava. Bioresour Bioprocess 8:25

Vanlalveni C, Lallianrawna S, Biswas A, Selvaraj M, Changmai B, Rokhum SL (2021) Green synthesis of silver nanoparticles using plant extracts and their antimicrobial activities: a review of recent literature. RSC Adv 11:2804

Veeramuthu L, Chen BY, Tsai CY, Liang FC, Venkatesan M, Jiang DH, Chen CW, Cai X, Kuo CC (2019) Novel stretchable thermochromic transparent heaters designed for smart window defroster applications by spray coating silver nanowire. RSC Adv 9:35786–35796

Wang S, Li T, Chen C, Kong W, Zhu S, Dai J, Diaz AJ, Hitz E, Solares SD, Li T, Hu L (2018) Transparent, anisotropic biofilm with aligned bacterial cellulose nanofibers. Adv Funct Mater 28:1707491

Wang Y, Chen L, Cheng H, Wang B, Feng X, Mao Z, Sui X (2020) Mechanically flexible, waterproof, breathable cellulose/polypyrrole/polyurethane composite aerogels as wearable heaters for personal thermal management. Chem Eng J 402:126222

Wu Z, Chen S, Wu R, Sheng N, Zhang M, Ji P, Wang H (2020) Top-down peeling bacterial cellulose to high strength ultrathin films and multifunctional fibers. Chem Eng J 391:123527

Wu H, Xie Y, Ma Y, Zhang B, Xia B, Zhang P, Qian W, He D, Zhang X, Li B-W, Nan C-W (2022) Aqueous MXene/Xanthan Gum hybrid inks for screen-printing electromagnetic shielding, joule heater, and piezoresistive sensor. Small 18:2107087

Yang W, Li J, Zhong Y, Qian H, Li Z, Hu Y (2013) Facile Cl–mediated hydrothermal synthesis of large-scale Ag nanowires from AgCl hydrosol. CrystEngComm 15:2598

Yu D, Yam VWW (2004) Controlled synthesis of monodisperse silver nanocubes in water. J Am Chem Soc 126:13200–13201

Yu B, Zhao Z, Fu S, Meng L, Liu Y, Chen F, Wang K, Fu Q (2019) Fabrication of PLA/CNC/CNT conductive composites for high electromagnetic interference shielding based on Pickering emulsions method. Compos A 125:105558–105567

Zhang K, Li Y, Zhou H, Nie M, Wang Q, Hua Z (2018) Polyurethane/ carbon fiber composite tubular electrode featuring three-dimensional interpenetrating conductive network. Carbon 139:999–1009

Zhang S, Liu H, Yang S, Shi X, Zhang D, Shan C, Mi L, Liu C, Shen C, Guo Z (2019) Ultrasensitive and highly compressible piezoresistive sensor based

on polyurethane sponge coated with a cracked cellulose nanofibril/silver nanowire layer. ACS Appl Mater Interfaces 11:10922–10932
Zhou B, Su M, Yang D, Han G, Feng Y, Wang B, Ma J, Ma J, Liu C, Shen C (2020a) Flexible MXene/Silver nanowire-based transparent conductive film with electromagnetic interference shielding and electro-photo-thermal performance. ACS Appl Mater Interfaces 12:40859–40869
Zhou B, Zhang Z, Li Y, Han G, Feng Y, Wang B, Zhang D, Ma J, Liu C (2020b) Flexible, robust, and multifunctional electromagnetic interference shielding film with alternating cellulose nanofiber and MXene layers. ACS Appl Mater Interfaces 12:4895–4905
Zhou B, Li Q, Xu P, Feng Y, Ma J, Liu C, Shen C (2021) An asymmetric sandwich structural cellulose-based film with self- supported MXene and AgNW layers for flexible electromagnetic interference shielding and thermal management. Nanoscale 13:2378–2388
Zhu S, Lou CW, Zhang S, Wang N, Li J, Feng Y, He R, Xu C, Lin JH (2022) Clean surface additive manufacturing of aramid paper-based electrically heated devices for medical therapy application. Surf Interfaces 29:101699
Zikmanis P, Kolesovs S, Ruklisha M, Semjonovs P (2021) Production of bacterial cellulose from glycerol: the current state and perspectives. Bioresour Bioprocess 8:116

Publisher's Note